

# On convection and mixing driven by sedimentation

By SILVANA S. S. CARDOSO AND ANDREW W. WOODS

Institute of Theoretical Geophysics, Department of Applied Mathematics and Theoretical Physics, University of Cambridge, Silver Street, Cambridge CB3 9EW, UK

(Received 13 July 1993 and in revised form 16 September 1994)

The sedimentation of small particles from a suspension and the concomitant release of light interstitial fluid may constitute a buoyancy source for the development of convective motions. When the dense suspension is emplaced beneath a stratified fluid, an intermediate convecting layer between the sedimenting front and the density gradient above gradually grows in depth by erosion of the overlying stratified fluid. Novel laboratory experiments involving sedimentation below a two-layer stratified region show that turbulent mixing and entrainment across the top density interface is significant for a broad range of the Richardson number. A simple theoretical model predicting the rate of erosion of the stratification above the convecting layer agrees well with these experiments. The model is then extended to include the case of an overlying continuous density gradient and compared successfully with both new experimental data and the original data of Kerr (1991). Owing to the effects of dispersion of grain sizes, small particles in the convecting fluid may lower the efficiency of the interfacial mixing by the turbulent eddies.

Our model calculations suggest that turbulent mixing and entrainment driven by sedimentation may be significant in the atmospheric and oceanic contexts, in both of which stratification is weak. Such mixing may also occur in molten magma chambers following the sedimentation of suspended crystals, and in this case it may suppress large-scale overturning events.

---

## 1. Introduction

When a dense suspension of small particles is emplaced below fluid of density greater than that of the interstitial fluid, the subsequent settling of the dense particles releases buoyant interstitial fluid which rises through the overlying layer and drives convection. If the overlying fluid is stratified, convection does not immediately extend throughout the layer but is confined to an intermediate region between the sedimenting front and the gradient above. This well-mixed convecting layer then gradually grows by erosion of the base of the density gradient.

An understanding of the behaviour of the interface at the top of the convecting region, and hence of the erosion process, is important since it arises in many phenomena in natural environments. In the atmosphere, for example, when precipitation or the descent of ice particles begins in a cloud, the release of the buoyant air with only the smaller drops or particles induces convection and mixing at the top of the cloud; this contributes significantly to the subsequent growth of the cloud (Ludlam 1980). Another situation is that found in dust storms; the interaction between sedimentation and convection during settling of the dust particles is relevant in determining the effects of the storm on the deepening of the lower mixed layer of the atmosphere. In the ocean, the sedimentation of particles transported by turbidity

currents constitutes a major mechanism for the mixing and ventilation of deep waters (Quadfasel, Kudrass & Frische 1990).

The original experimental study of Kerr (1991) focused upon mixing in very strong density gradients. Kerr suggested that the incorporation of overlying stratified fluid at the top of the convecting region may be dynamically passive: the continuous release of buoyant interstitial fluid decreases the density of the well-mixed convecting region and it deepens by encroaching upon the overlying gradient. However, in the ocean and atmosphere, the stratification is typically very weak so that the turbulent motions in the convecting layer may lead to some entrainment of the overlying light fluid. In this work we describe some new laboratory experiments which investigate such entrainment. These involve sedimentation below a two-layer stratification rather than a continuous gradient. This new configuration easily allows the study of the interface at the top of the convecting region for a broad range of the Richardson number, and allows comparison of the entrainment efficiency with that measured in other penetrative convection studies. There is also the advantage that at the beginning of an experiment, the convecting layer depth is already large and hence the initial period of time required for the establishment of vigorous convection is reduced. A few experiments involving sedimentation below a continuous density gradient were also performed. These extend the experimental study of Kerr (1991).

The work is organized as follows. In §2, we describe the experimental procedure. In §3, we develop a simple physical model for the mixing produced by sedimentation below a two-layer stratification; the turbulent entrainment at the top of the convecting layer is taken into account. In §4, the model predictions are compared with our experimental results. In §5, we extend this model to include the case of an overlying continuous density gradient. We analyse our new experimental data for this situation and also the experimental results of Kerr (1991). In §6, we describe the structure of the entraining interface and discuss its effect on the entrainment process. Finally, in §7, we consider the implications of our work in the geophysical context and draw some conclusions.

## **2. Experimental procedure**

The experiments were carried out in a Perspex tank  $20 \times 20 \text{ cm}^2$  in cross-sectional area and 50 cm deep. The tank was initially filled with two layers of fluid differing in density. A dense salt solution formed the bottom layer; the upper layer of less dense dyed fluid, either fresh water or a salt solution, was carefully added through a floating sponge. The thickness of the interface, determined by the intermediate intensity of colour, appeared to be about 0.5 cm. The typical depth of the upper layer was 10 cm.

The suspension was composed of fresh water and small silica carbide particles. The density of these particles is  $3.217 \text{ g cm}^{-3}$ . In order to reduce coagulation of the particles in the suspension, a small concentration of sodium hexametaphosphate, approximately 0.02% wt, was used. The experiments were initiated by carefully injecting the dense suspension at the bottom of the tank through a tube leading from a continuously stirred reservoir. The suspension was injected horizontally, beneath a small metal plate, to minimize the motion in the lower layer generated during input. Measurements of the position of the suspension/fluid interface and of the injected volume of suspension showed that there was very little mixing during input. The typical initial depth of the suspension layer was 11 cm. The positions of the sedimenting front and of the fluid/fluid interface were made clearly visible by suitable lighting and were then monitored in time.

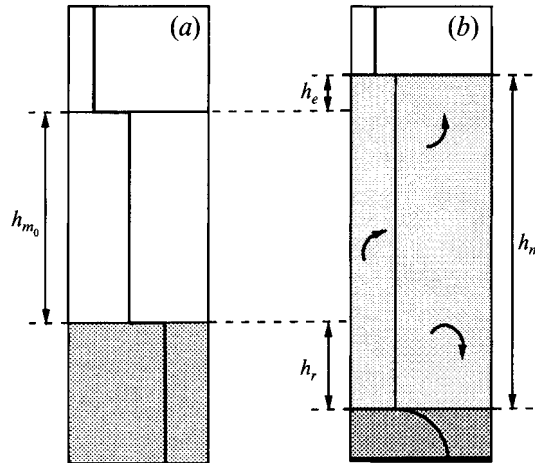


FIGURE 1. A schematic of sedimentation below a density step and the corresponding evolution of the bulk density profile. (a) The initial configuration. (b) As the particles settle, an intermediate well-mixed convecting layer grows at the expense of the underlying sedimenting region and by entrainment of the overlying buoyant fluid.

Expt	$d_p$ ( $\mu\text{m}$ )	$\rho_s$ ( $\text{g cm}^{-3}$ )	$\rho_{m_0}$ ( $\text{g cm}^{-3}$ )	$\rho_u$ ( $\text{g cm}^{-3}$ )	$h_{m_0}$ (cm)	$v_r$ ( $\text{cm min}^{-1}$ )	$X$	Symbol
1j	13	1.035	1.0152	1.0110	20	1.6	0.23	●
2j	13	1.027	1.0146	1.0086	20	1.6	0.17	■
3j	13	1.031	1.0181	1.0110	25	1.5	0.26	▲
4j	13	1.032	1.0157	0.9990	20	1.8	0.20	◆
5j	4	1.031	1.0153	1.0086	20	0.5	0.35	

TABLE 1. The experimental conditions for sedimentation below a density jump

Expt	$d_p$ ( $\mu\text{m}$ )	$\rho_s$ ( $\text{g cm}^{-3}$ )	$\rho_{u_0}$ ( $\text{g cm}^{-3}$ )	$N$ ( $\text{s}^{-1}$ )	$v_r$ ( $\text{cm min}^{-1}$ )	$X$	Symbol
1g	13	1.033	1.0243	0.539	1.5	0.15	●
2g	13	1.031	1.0250	0.694	1.7	0.18	■
3g	13	1.031	1.0246	0.619	1.8	0.20	▲

TABLE 2. The experimental conditions for sedimentation below a density gradient

Two samples of approximately 80 ml of the convecting layer fluid were withdrawn with a syringe, one at an early stage of the experiment and the other at the end. The fraction of sediment in each of these was determined by measuring the total mass of the sample and the mass of solid residue of sediment left after decantation and evaporation of the water. The very small particle concentrations in the convecting fluid required the collection of relatively large samples of the mixture, and hence only two such measurements were possible in each experiment.

The conditions for each experimental run are given in table 1. The fluids and particles used in the experiments were at room temperature ( $\approx 20^\circ\text{C}$ ). Two grades of particles were used, with mean diameter  $d_p$  of  $13\ \mu\text{m}$  and  $4\ \mu\text{m}$ . These particles are sufficiently small to settle at low Reynolds number in water and sufficiently big to settle at a velocity large enough to drive vigorous convection in the overlying fluid. The densities of the suspension,  $\rho_s$ , of the initial lower layer fluid,  $\rho_{m_0}$ , and of the upper layer fluid,  $\rho_u$ , were chosen so that turbulent entrainment effects at the interface between the

two layers of fluid would be measurable on the scale of our experiments. The initial depth of the lower layer,  $h_{m_0}$ , was sufficiently big for vigorous convection to develop soon after sedimentation began. Visual observations, as well as calculations (Hunt 1984), suggest that the lengthscale of the turbulent motions was of the order of 5–10 cm; this is substantially smaller than the horizontal length of the tank, and hence sidewall effects should be negligible.

A number of experiments with an overlying continuous density gradient were also carried out (table 2). In these the tank was initially filled with a linearly stratified salt solution produced by the double-bucket technique (Oster 1965). The injection of the suspension and the subsequent procedure was then the same as described above. The initial depth of the gradient region was approximately 30 cm. The buoyancy frequency of the stratification,  $N$ , was varied from 0.5 to 0.7 s<sup>-1</sup>. This range of values is limited by the depth of the tank used and by the density of the suspension. If the stratification is too weak, erosion of the whole upper layer will occur very rapidly, when the sedimenting front has fallen only a few centimetres; it is not possible to monitor the experiment any further without a much deeper tank. On the other hand, the density at the base of the original gradient,  $\rho_{u_0}$ , has to be smaller than that of the suspension so that the system is initially stable. However, very dense and hence concentrated suspensions cannot be used because particle–particle interactions become increasingly important with concentration. This places an upper limit on the value of  $N$ , since  $N^2 \propto (\rho_{u_0} - \rho_w)$ . The water in the suspension was dyed with food colouring in order to visualize the mixed layer fluid.

The rate of descent of the sedimenting front,  $v_r$ , and the mass fraction of the initial load of particles lifted into the convecting layer,  $X$ , were approximately constant during an experiment (see the Appendix). The average values of these are also shown in tables 1 and 2. Typically,  $X$  varied by about 15% for the 13  $\mu\text{m}$  diameter particles and 20% for the 4  $\mu\text{m}$  particles. The larger variation for the smaller particles is probably due to the greater effect of the distribution of particle sizes. The non-monotonic variation of  $X$  with  $v_r$  for the 13  $\mu\text{m}$  particles suggests that some particle coagulation occurred in the suspension. This does not affect the interpretation of our experimental results, as we shall see later. We note that the magnitude of  $v_r$  is significantly larger than the Stokes' free-fall velocity. This is a result of both the dispersion of particle sizes in the suspension and the presence of the overlying less-dense fluid, as will be explained in the next section.

### 3. Theoretical description

The evolution of an experiment is shown schematically in figure 1. The initial configuration is a two-layer stratified system underlain by a suspension. As the particles sediment, buoyant interstitial fluid is released and rises into the lower overlying layer, driving convection. These convective motions are responsible for the entrainment at the top of this convecting layer and depend upon the buoyancy flux released by the sedimenting front of particles.

The motion of the sedimenting front has been studied by Huppert *et al.* (1991) and Kerr & Lister (1992). The experimental work of these authors showed that the natural dispersion of the sizes of the particles in the suspension is important in determining the descent velocity of the sedimenting front. Because the particles settle with a range of velocities, the suspension bulk density becomes smoothly stratified. Near the top there is only interstitial fluid, whereas at intermediate depths smaller particles remain in suspension and at the base all particle sizes are present. At the top of the suspension,

the bulk density of the interstitial fluid and suspended small particles is less than that of the overlying fluid and this buoyant layer of dilute suspension convects away.

Those authors noted further that as the buoyant part of the suspension in the boundary layer above the interface detaches and rises into the overlying fluid, it carries some of the underlying dense suspension. The efficiency of this entrainment was observed to vary with the intensity of convection. Based on buoyancy arguments, Huppert *et al.* (1991) presented theoretical upper and lower bounds on the amount of particle entrainment into the overlying convecting layer and hence on the velocity of the sedimenting front. In practice, they found that the entrainment is weak but non-negligible. However, no complete theoretical description exists for this entrainment effect. Therefore in order to make quantitative comparisons between our experimental and theoretical results concerning the dynamics of the interface at the top of the convecting region, we shall use as an input to our model the measured experimental value for the fraction of sediment and hence the buoyancy flux supplied to the convecting layer.

*Dynamics of the interface at the top of the convecting region*

In many of the previous experiments (Huppert *et al.* 1991; Kerr & Lister 1992) and in the experiments described in this paper, the variation of the velocity of the sedimenting front was small. We shall therefore make the simplifying assumption that it is constant. This implies that the fraction of sediment lifted, as a result of both the detachment of the buoyant dilute suspension and of the entrainment of dense suspension from below, is also approximately constant during an experiment (see the Appendix).

The simplification that a constant fraction of the original sediment, say  $X$ , is lifted by the rising buoyant fluid allows a simple description of the sedimentation and mixing processes. As the sedimenting front falls, buoyant particle-laden fluid of density

$$\rho_r = \frac{\rho_p}{(\rho_s - \rho_w)X + \rho_p - \rho_s} (\rho_s - \rho_w) X + \frac{\rho_p - \rho_s}{(\rho_s - \rho_w)X + \rho_p - \rho_s} \rho_w \tag{3.1}$$

will be released. Here  $\rho_p$ ,  $\rho_s$  and  $\rho_w$  are the actual densities of the solid particles, of the suspension and of clear water, respectively. We assume that the density of the mixture of fluid and solid particles varies linearly with the volume fraction of its components, i.e. that contraction or expansion effects during mixing are negligible. In the limit of very low particle concentrations ( $\rho_s \sim \rho_w$ ) and for relatively dense solid particles ( $\rho_p \gg \rho_w$ ), the equation above may be simplified and written as

$$\rho_r = (\rho_s - \rho_w) X + \rho_w. \tag{3.2}$$

The depth of the mixed layer increases with time at the expense of both the underlying sedimenting region and the overlying layer of light fluid. After some time has passed, the sedimenting front has descended a distance  $h_r$  and the depth of light fluid that has been entrained into the mixed layer is  $h_e$  (figure 1). Conservation of mass of the mixed layer requires

$$\rho_m h_m = \rho_r h_r + \rho_{m_0} h_{m_0} + \rho_u h_e, \tag{3.3}$$

with its depth given by

$$h_m = h_r + h_{m_0} + h_e, \tag{3.4}$$

where subscripts  $m$  and  $u$  refer to the mixed and upper layers of fluid, respectively, and 0 denotes initial conditions.

If the sedimenting front descends at a velocity  $v_r = dh_r/dt$ , the buoyancy flux driving convection is

$$B_r = g \frac{\rho_m - \rho_r}{\rho_r} v_r. \quad (3.5)$$

By analogy with other situations of penetrative convection, the rate of entrainment of light fluid at the top of the convecting layer may be described by

$$\frac{dh_e}{dt} = c_1 \frac{B_r}{b_i}, \quad (3.6)$$

where  $b_i$  is the buoyancy difference across the interface,  $b_i = g(\rho_m - \rho_u)/\rho_r$  (Zilitinkevich 1991; Fernando 1991). The most comprehensive review of empirical estimates for the constant  $c_1$  suggest that it lies in the range 0.1 to 0.3 (Zilitinkevich 1991). The relation (3.6) is a simple parameterized model of turbulent entrainment, based on the assumption that a constant fraction of the kinetic energy made available by the buoyancy flux driving convection is converted into potential energy of the mixed layer. Internal-wave radiation and wave-breaking effects have been neglected; the former occurs only when the overlying fluid is stratified and the latter is negligible for low values of the Richardson number,  $Ri \sim 1$  (E & Hopfinger 1986). Equation (3.6) is equivalent to an inverse Richardson number law for the entrainment rate. The Richardson number is defined here as  $Ri = b_i h_m / \omega^2$ , with the convective velocity scale  $\omega$  given by  $\omega = (B_r h_m)^{1/3}$ .

The evolution of the depth of the convecting layer may be determined from (3.3)–(3.6). The depth of entrained upper fluid is related to the distance fallen by the sedimenting front by

$$\frac{dh_e}{dh_r} = c_1 \frac{\rho_m - \rho_r}{\rho_m - \rho_u}. \quad (3.7)$$

Integrating this equation with initial conditions  $h_r = 0$ ,  $h_e = 0$  leads to

$$h_e = h_{m_0} \frac{\rho_{m_0} - \rho_r}{\rho_u - \rho_r} \left( -1 + \left( 1 - \frac{\rho_u - \rho_r}{\rho_{m_0} - \rho_u} \frac{h_r}{h_{m_0}} \right)^{-c_1} \right), \quad \rho_r \neq \rho_u, \quad (3.8a)$$

$$h_e = c_1 h_r, \quad \rho_r = \rho_u. \quad (3.8b)$$

The evolution of the system with time may be obtained by substituting in this equation the dependence of  $h_r$  on  $t$ . For example, in the simplest case of a constant sedimentation velocity,  $h_r = v_r t$ . In order to compare the predictions of this simple model with our experimental results, it is convenient to define the non-dimensional variables

$$h_e^* = \frac{h_e}{h_{m_0}} \frac{\rho_u - \rho_r}{\rho_{m_0} - \rho_r}, \quad h_r^* = \frac{h_r}{h_{m_0}} \frac{\rho_u - \rho_r}{\rho_{m_0} - \rho_u}, \quad (3.9a, b)$$

where  $\rho_r \neq \rho_u$ . Equation (3.8a) may then be written in a general form as

$$h_e^* = -1 + (1 - h_r^*)^{-c_1}. \quad (3.10)$$

#### 4. Comparison of theoretical description and experimental results

The fraction of sediment lifted,  $X$ , is required as an input to our model, in order to calculate the buoyancy flux driving convection,  $B_r$  (see (3.6)). The value of  $X$  may be obtained either by direct experimental measurement or, alternatively, from the

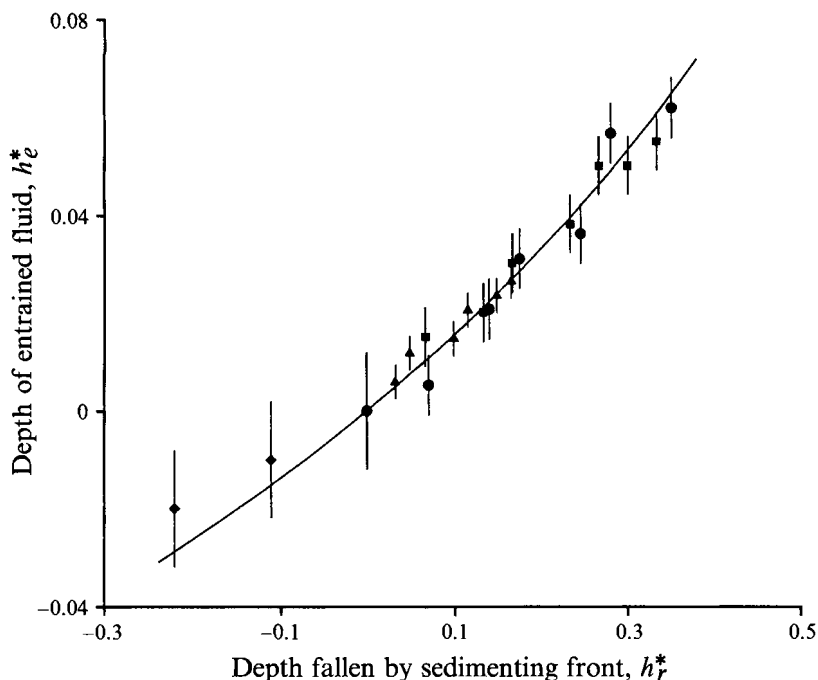


FIGURE 2. The results for sedimentation below a density step. Comparison of the entrainment model prediction with the experimental data of the depth of entrained upper fluid as a function of the depth fallen by the sedimenting front. Experimental conditions are given in table 1.

measurement of the sedimenting velocity and knowledge of the distribution of the settling velocities of the particles (see Kerr 1991). The latter method is, however, inaccurate when coagulation of particles occurs in the suspension. We have therefore used the value of  $X$  measured directly in each experiment (see §2 and the Appendix).

In figure 2, we present the results for the two-layer stratification experiments. The experimental data for the depth of entrained upper fluid as a function of the distance fallen by the sedimenting front is shown in non-dimensional form. The theoretical prediction of (3.10) is also graphed. It may be seen that the agreement between the experimental results and the model predictions is very good. The value of the entrainment constant  $c_1$  (equation (3.6)) giving the best description of our experimental results was estimated by linear regression. A value of  $0.15 \pm 0.02$  was obtained. This value is within the range reported in previous works on penetrative convection mentioned above (e.g. Zilitinkevich, 1991).

In figure 3, a sequence of photographs of the interface at the top of the convecting layer in experiment 3j is shown. As sedimentation in the suspension begins, the buoyant interstitial fluid, laden with small particles, rises into the layer of fluid above in the form of single, non-interacting plumes. These plumes impinge on and distort the interface, generating a wave-like motion. After this initial period, the intermediate layer begins to convect more vigorously and becomes homogeneous. The interface at the top of the convecting region is then periodically disrupted by turbulent eddies which entrain and mix buoyant fluid from the upper layer into the convecting fluid below. In the last photograph, the structure of the interface, with cusps and domes, resembles that observed in the entrainment zone for penetrative convection. The value of the Richardson number here is 2.8.

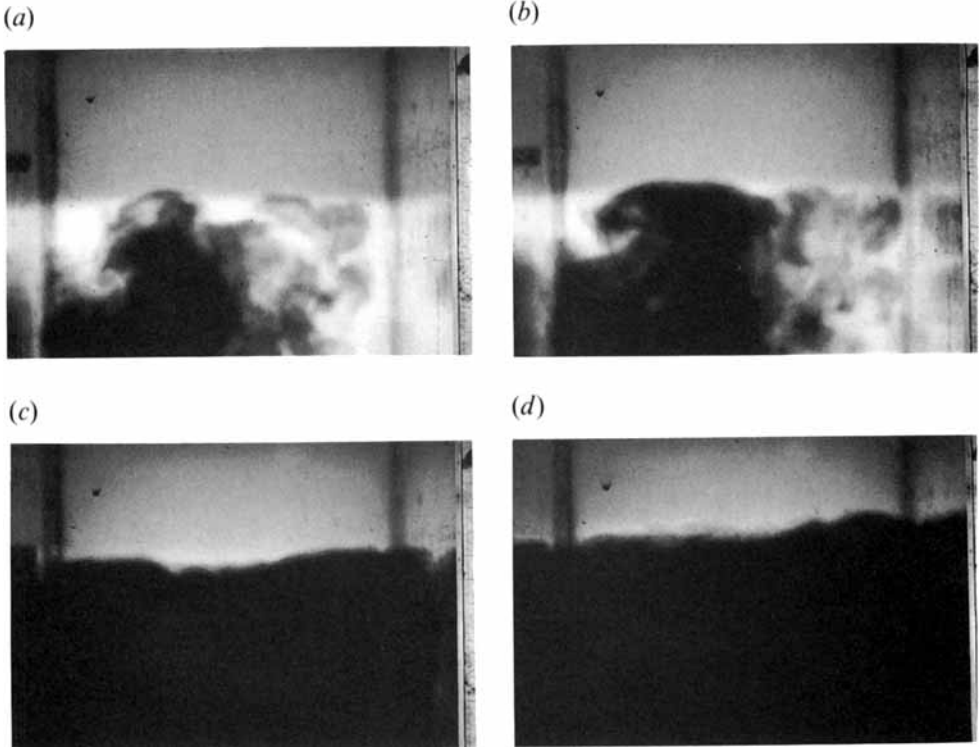


FIGURE 3. Structure of the interface at the top of the convecting layer when the interstitial fluid in this layer is more dense than the overlying fluid. The Richardson number here varies from 3.4 to 2.8. The fluid in the upper layer has been dyed for visualization. The photographs are of experiment 3j at times (a) 0 s, (b) 6 s, (c) 3 min and (d) 6 min.

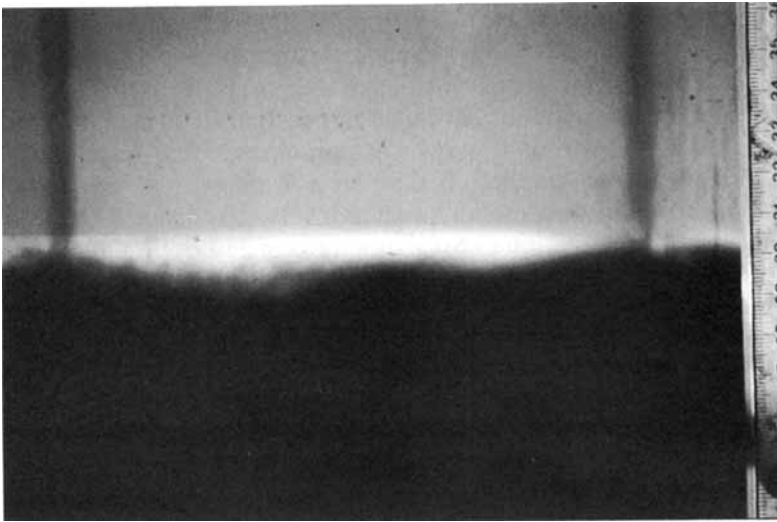


FIGURE 4. Aspect of the interface at the top of the convecting layer for a Richardson number of 11. (The interstitial fluid in the convecting layer is more dense than the overlying fluid.) The fluid in the upper layer has been dyed for visualization. Note the thin film of lower-layer white fluid which remains uneroded owing to the strong stratification at the inversion.

At higher values of the Richardson number, the distortion of the interface is less pronounced and the observed entrainment effect is smaller. In experiment 4j the Richardson number varied from 7.9 to 6.6. The corresponding experimental results are represented as diamonds in figure 2. Wave-breaking effects are expected to become significant at these relatively high values of  $Ri$ , and may account for the somewhat lower efficiency of entrainment observed in this experiment (E & Hopfinger 1986). However, within experimental accuracy, there is still agreement with the theoretical curve.

At still higher Richardson number, investigated in experiment 5j, the convective motions in the intermediate layer are unable to distort the interface and it remains flat. Figure 4 shows the structure of the interface for a Richardson number of approximately 11. No entrainment was observed in this case. Our model predicts a maximum entrainment depth of 1 cm for this experiment. It is thought that this larger difference between the experimental results and the theoretical predictions is due to the smaller buoyancy flux driving convection. Indeed, the particles chosen for this experiment were smaller and hence settled at a much lower velocity. Moreover the fraction of sediment lifted was larger. The resulting smaller buoyancy flux might not have been sufficient to develop full turbulent convection. This interpretation is supported by our laboratory observations that the convection in the intermediate layer did not appear to be as vigorous in this case as in the previous experiments.

### 5. Sedimentation below a density gradient

As mentioned above, the experiments of Kerr (1991) involved sedimentation of particles from a dense suspension emplaced below a stable density gradient of density greater than that of the interstitial fluid. It is interesting to analyse this situation since it is frequently encountered in nature. We extend our previous theoretical description to include this case.

Consider the schematic in figure 5. The upper layer is linearly stratified with buoyancy frequency  $N$ . After some time has evolved, a depth  $h_e$  of overlying stably stratified fluid has been mixed into the convecting layer and the density of the fluid being entrained is

$$\rho_u = \rho_{u_0} - N^2 \frac{\rho_r}{g} h_e, \quad (5.1)$$

where  $\rho_{u_0}$  is the density at the base of the original gradient region before erosion. Conservation of mass of the mixed layer is expressed by

$$\rho_m h_m = \rho_r h_r + \left( \rho_{u_0} - N^2 \frac{\rho_r h_e}{g} \right) h_e, \quad (5.2)$$

with 
$$h_m = h_r + h_e. \quad (5.3)$$

We need now to quantify the rate of erosion of the overlying density gradient by the turbulent convective motions in the mixed layer. Although internal-wave radiation may occur in the presence of the stable density gradient, this effect is small when the gradient Richardson number  $Ri_g = \frac{1}{2} N^2 h_m^2 / \omega^2 \leq 1$  (Zilitinkevich 1991). This is the case in our study, and also in the oceans and atmosphere. We may therefore neglect this energy loss and use the entrainment law (3.6).

The system of equations (3.5), (3.6) and (5.1)–(5.3) requires numerical solution. A

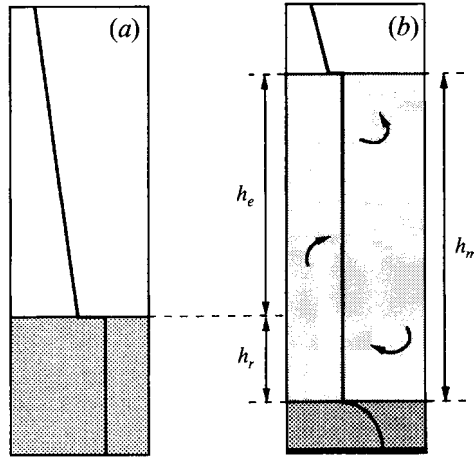


FIGURE 5. A schematic of sedimentation below a continuous density gradient and the corresponding evolution of the bulk density profile. (a) The initial configuration. (b) As the particles settle, an intermediate well-mixed convecting layer grows at the expense of the underlying sedimenting region and by erosion of the overlying stratified region.

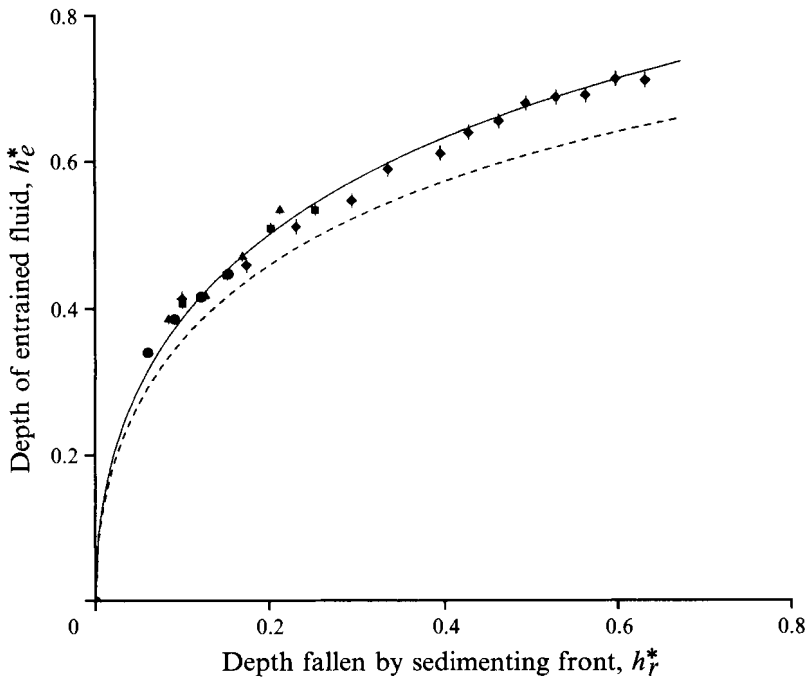


FIGURE 6. The results for sedimentation below a constant density gradient. Comparison of the predictions of the enainment model (solid line) and encroachment model (dashed line) with the experimental data for the depth of entrained upper fluid as a function of the depth fallen by the sedimenting front. Experimental conditions are given in table 2. The experimental data of Kerr (1991) are shown as diamonds.

Runge-Kutta integrating scheme was used, with the initial condition given by the asymptotic solution for  $h_r \sim 0$ :

$$\rho_m = \rho_{u_0}, \quad h_e = \left( 2c_1 \frac{g}{N^2} \frac{\rho_{u_0} - \rho_r}{\rho_r} h_r \right)^{1/2}. \quad (5.4a, b)$$

The theoretical predictions of this model are compared with our experimental results for sedimentation below a continuously stratified region in figure 6. The depth of entrained upper fluid,  $h_e$ , and the distance fallen by the sedimenting front,  $h_r$ , have both been non-dimensionalized on the lengthscale

$$H = \frac{g}{N^2} \frac{\rho_{u_0} - \rho_r}{\rho_r}, \quad (5.5)$$

i.e.  $h_e^* = h_e/H$  and  $h_r^* = h_r/H$ . Comparison of our experimental data with the theoretical prediction suggests the entrainment constant  $c_1$  lies in the range  $0.07 \pm 0.02$ . This value is somewhat smaller than that obtained previously for the case of a two-layer stratification. We propose a physical explanation for this difference in the next section.

It is interesting to compare the predictions of the entrainment model above with those obtained for a simple encroachment process. In the latter case, the density step in the entrainment zone grows very slowly and  $\rho_m \sim \rho_u(h_e)$  even at large times. From (5.1)–(5.3), we have in this limit

$$h_e = h_r \left( -1 + \left( 1 + \frac{2g}{N^2 h_r} \frac{\rho_{u_0} - \rho_r}{\rho_r} \right)^{1/2} \right). \quad (5.6)$$

In non-dimensional form,

$$h_e^* = h_r^* \left( -1 + \left( 1 + \frac{2}{h_r^*} \right)^{1/2} \right). \quad (5.7)$$

This solution is represented as a dashed curve in figure 6. It may be seen that the effect of turbulent entrainment, though not as strong as in the two-layer stratification, is nevertheless significant.

We now compare the experimental results of Kerr (1991) with the entrainment model. The experimental data presented in figure 4(a) of Kerr (1991) suggest that to a good approximation, the sedimenting velocity was constant. Combining this velocity and the distribution of settling velocities of the particles used (figure 3 of Kerr & Lister 1992), we estimate a value of 0.15 for the fraction of sediment lifted,  $X$ . Although there may have been some evolution of  $X$  during the experiment (see the Appendix), this was very small and so, to evaluate the role of entrainment of the overlying fluid, we have used the simplest assumption consistent with the data: that  $v_r$  and hence  $X$  are constant. A more complex empirical description of the velocity of the sedimenting front is not warranted by the data; we note that there is no theoretical model to predict this velocity. The experimental data of Kerr (1991) is represented as diamonds in figure 6. The agreement with the prediction of the present model, using the entrainment coefficient  $c_1$  of 0.07 which was determined independently from our constant-gradient experiments, is good. We therefore suggest that in the experiments of Kerr there was some entrainment at the top of the convecting layer. The stratification of the upper layer, although relatively large ( $N = 0.7 \text{ s}^{-1}$ ), was probably insufficient for an extreme restriction of the entrainment process. We note that although the theoretical predictions of Kerr (1991) for the rate of ascent of the top interface assuming an encroachment process also agreed well with the experimental data (his figure 4b), the actual velocity of descent and hence buoyancy flux released at the sedimenting front was in fact smaller than that computed from his theory (figure 4a in Kerr 1991) and we suggest that this may have compensated for the neglect of turbulent entrainment at the top of the convecting layer.

## 6. Structure of the entrainment interface

In the continuous stratification experiments, the structure of the interface between the convecting region and the uneroded gradient appeared to be very different from that observed in the two-layer stratification experiments (cf. figure 3). In the presence of the overlying gradient, the interface was diffuse and the upper part consisted of vertical narrow protrusions of sediment-rich fluid intruding into the gradient (figure 7). These finger-like elements were occasionally disrupted by large blobs arising from the convecting region. Kerr (1991) suggested that these protrusions develop from a local gravitational instability. In the mixed region, the convective velocities are much greater than the settling velocities of the particles (typically, by two orders of magnitude in our experiments) and hence the particles are carried around by the fluid. However, near the top of the mixed region, the vertical convective velocities decrease to values comparable to the rate of erosion of the overlying density gradient, and thus some of the suspended particles may sediment, provided their settling velocity,  $v_s$ , is greater than the rate of erosion. As these particles fall, a thin layer of depleted suspension, with decreased bulk density, is left at the top of the mixed layer. This thin layer grows until it becomes unstable and breaks up to form small buoyant protrusions. The subsequent development into longer finger-like elements, as described above, is possible only if their ascent speed,  $v_p$ , is larger than the rate of turbulent erosion of the overlying fluid. At steady state, the conservation of mass of this layer of particle-depleted buoyant suspension requires that  $v_p \sim (A/A_p)v_s$ , where  $A$  is the total cross-sectional area of the tank and  $A_p$  is the cross-sectional area covered with protrusions. Since  $A/A_p > 1$ , then if the settling velocity of the particles is greater than the erosion rate, the particles fall out at the top of the convecting layer and protrusions will grow.

In our constant-gradient experiments, the Stokes velocity of the particles,  $v_s$ , is of the order of the erosion rate during most of the experiment. Therefore, the larger particles (or coagules of particles) are able to fall out and lead to the formation of weak, particle-laden buoyant protrusions. In the two-layer stratification experiments rising protrusions were not seen. This is because the density of the fluid in the convecting layer is greater than that of the overlying fluid during most of each experiment. Therefore, even if all the particles fall out, the fluid at the top of the convecting layer is still stable. It is only near the end of some of the experiments that the density of the fluid in the convecting layer becomes smaller than that of the overlying fluid. However, the Richardson number of the interface is then small; the turbulent eddies impinging on it have large overshoots and the rate of erosion of the overlying layer increases. These effects suppress the growth of protrusions.

The diffuse nature of the interface at the top of the convecting layer observed in the case of a continuous stratification may, in general, affect the turbulent entrainment process. Indeed, some interaction between the two processes is expected for sufficiently strong finger-type convection at the top of the growing convecting layer, such that the vertical lengthscale of these finger elements is of the same order as the thickness of the turbulent entrainment layer. The protrusions ultimately stop growing when they become neutrally buoyant, owing either to the presence of a background stratification and/or to diffusion of their buoyancy anomaly. In very weakly stratified or neutral environments, diffusion has the dominant effect in determining the final length of the protrusions. However, in strongly stratified environments, the fingers may rise to their neutral buoyancy level in relatively short timescales so that the effect of diffusion is negligible. Simple calculations suggest that the latter effect dominates in both the present study and in that of Kerr (1991). In our experiments (§5), the rising protrusions

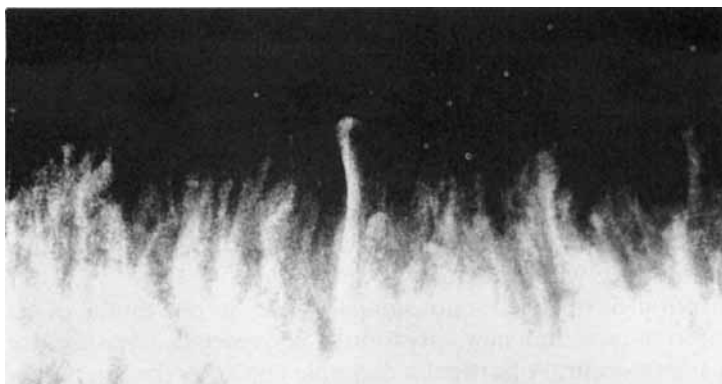


FIGURE 7. Structure of the interface at the top of the convecting layer when the interstitial fluid in this layer is less dense than the overlying undisturbed fluid (from Kerr 1991).

penetrated about 1 cm into the upper layer; in Kerr's experiments the protrusions penetrated further, 1–2 cm. The thickness of the turbulent entrainment layer may be roughly estimated as being 25% of the depth of the convecting layer (Deardorff, Willis & Stockton 1980; Hunt 1984), which corresponds to 5–10 cm. However, our visual observations suggest somewhat lower values, 3–4 cm. Owing to this similarity of lengthscales, the buoyant protrusions may promote a little mixing at the top of the convecting layer, changing both the local density step that turbulent entrainment creates (see figure 5) and the background density gradient in the vicinity. We therefore suggest that such a diffuse interface may account for the difference between the values of the entrainment constant  $c_1$  found in our experiments; a value of 0.07 was measured in the constant-gradient experiments, in contrast to 0.15 for the two-layer stratification experiments. Note that in the presence of weak stratification, such as found in the oceans and atmosphere, and/or for small particle concentrations, the density of the convecting fluid will actually be greater than that of the overlying gradient. The structure of the interface would then be similar to that observed in our two-layer stratification experiments.

## 7. Conclusions

In this work we have extended the recent investigations by Kerr & Lister (1992) on convection driven by particle sedimentation. When a suspension is emplaced beneath a stratified fluid, the subsequent settling of the dense particles may lead to the formation of an intermediate well-mixed convecting layer. This well-mixed layer grows in depth at the expense of both the sedimenting region and of the overlying stratified region. We have focused here upon the behaviour of the interface at the top of the convecting layer.

Some new laboratory experiments using a two-layer stratification were performed. These extend the previous experimental results of Kerr (1991) for an overlying continuous density gradient. A simple physical model predicting the rate of erosion of the stratification above the convecting layer was derived. This model takes into account the turbulent entrainment at the top of the convecting region; this effect had previously been neglected on the assumption that it was small. Our model predictions compare well with both the new experimental data and that of Kerr (1991) and suggest that entrainment may occur in many natural environments.

We have noted that the structure of the interface at the top of the convecting region may vary depending upon whether the convecting fluid density is greater or smaller than that of the overlying fluid. In the former case, waves, cusps and domes are clearly visible in the turbulent entrainment zone, resembling observations in thermal convection studies. In the latter situation, the interface is much more diffuse owing to the development of finger-like vertical protrusions. This local convection, if sufficiently strong, may interact with and affect the turbulent mixing at the interface. It was suggested that in many natural situations, where stratification is relatively weak, the former type of interface will develop.

The incorporation of turbulent entrainment effects in our model of sedimentation-driven convection shows that new, previously unexpected, dynamical evolutions of natural systems may occur. A particular example concerns the mixing induced by the sedimentation of suspended crystals in a cooling stratified magma chamber. It has been suggested (Huppert 1986; Koyaguchi *et al.* 1990) that when the crystals grow sufficiently large and settle to the bottom of the chamber, the release of the light interstitial magma below a two-layer stratification may lead to a large decrease in the density of the lower layer with eventual overturning and total mixing. However, we note that, somewhat counterintuitively, turbulent entrainment at the interface between the magma layers may allow the stratified state of the reservoir to be preserved. Indeed, if the entrainment of the overlying light layer at the upper interface is significant, the light crystal-depleted magma released through sedimentation at the sedimenting front may be unable to cause a sufficient reduction of the density of the lower layer for overturn. We should also mention that for such deep reservoirs and high-viscosity fluids, the thickness of the turbulent entrainment layer will always significantly exceed the vertical lengthscale of the convective protrusions which might develop at the top of the convecting region. Hence, the interfacial turbulent mixing process will not be affected by this weak local instability.

We conclude by noting that a global model of sedimentation-driven convection in a stratified region should include both the effects of the change in sedimentation velocity with the buoyancy flux driving convection and that of turbulent mixing and entrainment at the base of the stratified fluid. A complete theoretical description of the former effect and hence of the dynamic behaviour of a sedimenting interface is still needed.

We would like to thank Dr Ross C. Kerr for his kind supply of the photograph in figure 7 and both Dr John R. Lister and Dr Ross C. Kerr for useful discussions about this problem. We are also grateful to the anonymous reviewers for their very helpful suggestions. This work has been supported by the Commission of the European Communities Science Programme through grant B/910076.

### **Appendix. Sedimenting velocity and fraction of sediment lifted**

As mentioned in §2, in each experiment we made two independent determinations of the fraction of sediment lifted by the buoyant interstitial fluid,  $X$ . The results differed by less than 15% and we have therefore made the approximation that this quantity is constant during an experiment. It is however important to confirm the constancy of  $X$  with our more exhaustive velocity measurements. When the distribution of particle sizes has a significant variance about its mean, the observed sedimenting velocity,  $v_s$ , varies significantly with the fraction of sediment lifted. Therefore, variations in  $X$  will

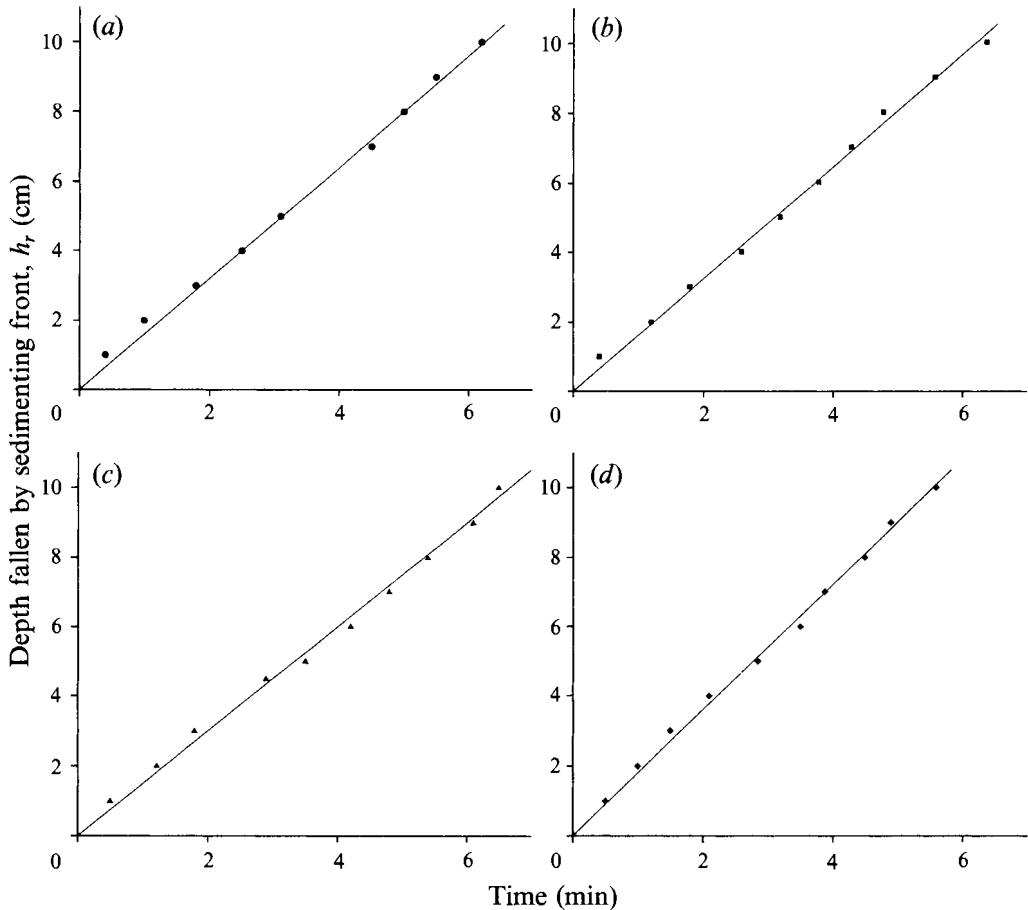


FIGURE 8. Depth fallen by the sedimenting front as a function of time for the two-layer stratification. (a-d) Expts 1j-4j respectively. Experimental conditions are given in table 1.

result in variations in  $v_r$  (see Kerr & Lister 1992). The particles used here, and indeed most natural samples, have distributions of this form.

In figure 8, the position of the sedimenting front is shown as a function of time for the two-layer stratification experiments. The descent velocity may be seen to be approximately constant in each experiment. This is consistent and confirms our findings of an approximately constant value for  $X$ . Figure 9 shows the sedimenting velocity measurements for the continuous stratification experiments. In this case it was again approximately constant, and hence we may infer that  $X$  was constant in each experiment. Average values of  $v_r$  were obtained by regression and are presented in tables 1 and 2. Note that the model presented here is actually independent of the magnitude of the sedimenting velocity. This velocity determines only the timescale of the process.

#### REFERENCES

- DEARDORFF, J. W., WILLIS, G. E. & STOCKTON, B. H. 1980 Laboratory studies of the entrainment zone of a convectively mixed layer. *J. Fluid Mech.* **100**, 41-64.
- E, X. & HOPFINGER, E. J. 1986 On mixing across an interface in a stably stratified fluid. *J. Fluid Mech.* **166**, 227-244.

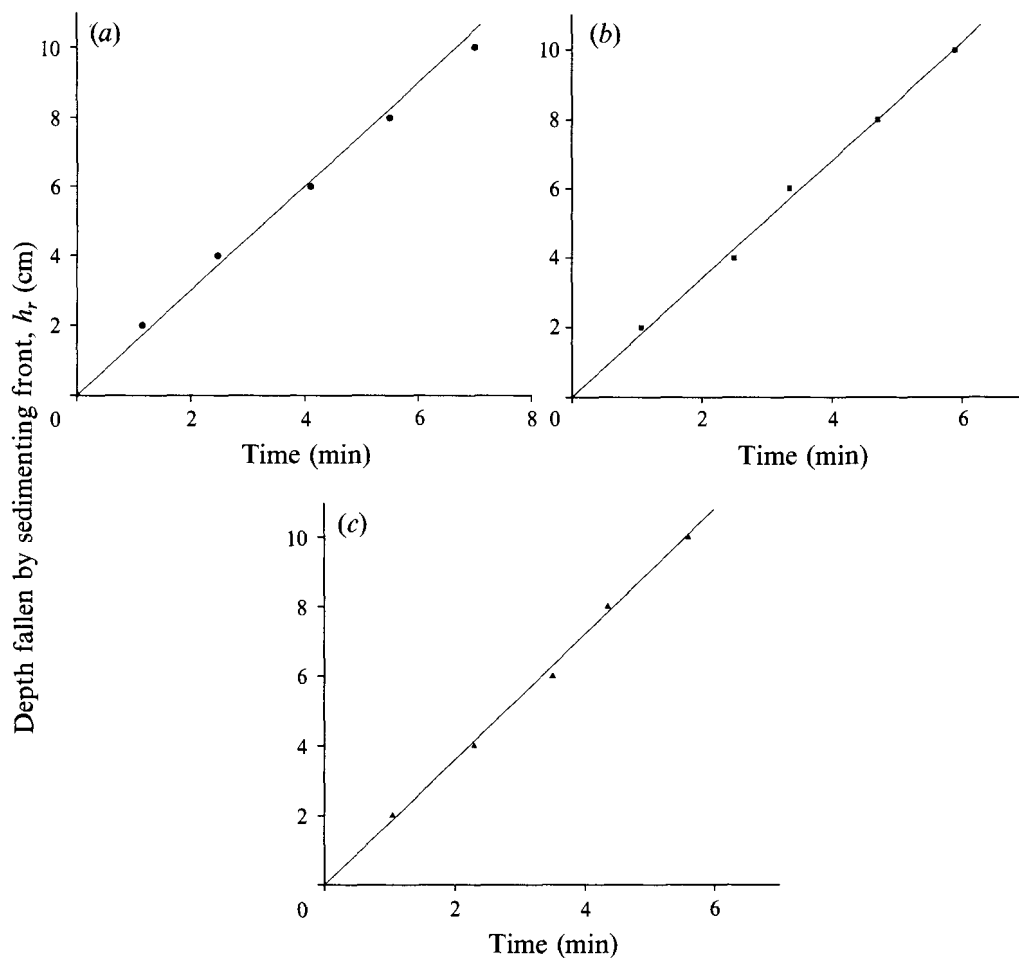


FIGURE 9. Depth fallen by the sedimenting front as a function of time for the constant-gradient stratification. (a-c) Expts 1g-3g respectively. Experimental conditions are given in table 2.

- FERNANDO, H. J. S. 1991 Turbulent mixing in stratified fluids. *Ann. Rev. Fluid Mech.* **23**, 455-493.
- HUNT, J. C. R. 1984 Turbulence structure in thermal convection and shear-free boundary layers. *J. Fluid Mech.* **138**, 161-184.
- HUPPERT, H. E. 1986 The intrusion of fluid mechanics into geology. *J. Fluid Mech.* **173**, 557-594.
- HUPPERT, H. E., KERR, R. C., LISTER, J. R. & TURNER, J. S. T. 1991 Convection and particle entrainment driven by differential sedimentation. *J. Fluid Mech.* **226**, 349-369.
- KERR, R. C. 1991 Erosion of a stable density gradient by sedimentation-driven convection. *Nature* **353**, 423-425.
- KERR, R. C. & LISTER, J. R. 1992 Further results for convection driven by the differential sedimentation of particles. *J. Fluid Mech.* **243**, 227-245.
- KOYAGUCHI, T., HALLWORTH, M. A., HUPPERT, H. E. & SPARKS, R. S. J. 1990 Sedimentation of particles from a convecting fluid. *Nature* **343**, 447-450.
- LUDLAM, F. H. 1980 *Clouds and Storms*, pp. 129-181. The Pennsylvania State University Press.
- OSTER, G. 1965 Density gradients. *Sci. Am.* **213**, 70-76.
- QUADFASSEL, D., KUDRASS, H. & FRISCHE, A. 1990 Deep-water renewal by turbidity currents in the Sulu Sea. *Nature* **348**, 320-322.
- ZILITINKEVICH, S. S. 1991 *Turbulent Penetrative Convection*, pp. 1-77. Avebury Technical.